



Article (refereed) - postprint

McCarthy, Gerard D.; Haigh, Ivan D.; Hirschi, Joël J.-M.; Grist, Jeremy P.; Smeed, David A.. 2015 Ocean impact on decadal Atlantic climate variability revealed by sea-level observations. *Nature*, 521 (7553). 508-510. [10.1038/nature14491](https://doi.org/10.1038/nature14491)

© 2015 Nature Publishing Group

This version available at <http://nora.nerc.ac.uk/510937/>

NERC has developed NORA to enable users to access research outputs wholly or partially funded by NERC. Copyright and other rights for material on this site are retained by the rights owners. Users should read the terms and conditions of use of this material at <http://nora.nerc.ac.uk/policies.html#access>

NOTICE: this is the author's version of a work that was accepted for publication in *Nature*. Changes resulting from the publishing process, such as peer review, editing, corrections, structural formatting, and other quality control mechanisms may not be reflected in this document. Changes may have been made to this work since it was submitted for publication. A definitive version will be published in *Nature* [10.1038/nature14491](https://doi.org/10.1038/nature14491)

Contact NOC NORA team at
publications@noc.soton.ac.uk

1 **Ocean impact on decadal Atlantic climate variability revealed by sea-level**
2 **observations***

3

4 Gerard D. McCarthy¹, Ivan D. Haigh², Joël J.-M. Hirschi¹, Jeremy P. Grist¹ and David A.
5 Smeed¹

6

7 ¹National Oceanography Centre, University of Southampton Waterfront Campus,
8 European Way, Southampton, SO14 3ZH, UK

9

10 ²Ocean and Earth Science, National Oceanography Centre, University of Southampton,
11 Waterfront Campus, European Way, Southampton, SO14 3ZH, UK

12

13 **Decadal variability is a notable feature of the Atlantic Ocean and the climate of the**
14 **regions it influences. Prominently, this is manifested in the Atlantic Multidecadal**
15 **Oscillation (AMO) in sea-surface temperatures (SSTs). Positive (negative) phases of**
16 **the AMO coincide with warmer (colder) North Atlantic SSTs. The AMO is linked**
17 **with decadal climate fluctuations such as Indian and Sahel rainfall¹, European**
18 **summer precipitation², Atlantic hurricanes³ and variations in global temperatures⁴.**
19 **It is widely believed that ocean circulation drives the phase changes of the AMO by**
20 **controlling ocean heat content⁵. However, there are no direct observations of ocean**
21 **circulation of sufficient length to support this, leading to questions about whether**

* This is the author's post-print version. Some text may vary from the final accepted version

22 **the AMO is controlled from another source⁶. Here we provide for the first time**
23 **observational evidence of the widely hypothesized link between ocean circulation**
24 **and the AMO. We take a new approach using sea level along the east coast of the**
25 **United States to estimate ocean circulation on decadal timescales. We show that**
26 **ocean circulation responds to the first mode of Atlantic atmospheric forcing, the**
27 **North Atlantic Oscillation (NAO), through circulation changes between the**
28 **subtropical and subpolar gyres—the intergyre region⁷. These circulation changes**
29 **impact the decadal evolution of North Atlantic heat content and, consequently, the**
30 **phases of the AMO. The Atlantic overturning circulation is declining⁸ and the AMO**
31 **is moving to a negative phase. While this may offer brief respite from the persistent**
32 **rise of global temperatures⁴, this link between circulation and sea-level implies that**
33 **it is no coincidence that sea-level rise along the northeast coast of the United States**
34 **is also accelerating^{9,10}.**

35

36 The difficulty in linking ocean circulation changes to decadal climate variations lies in
37 the fact that long observational records of ocean transports are rare. Measurements such
38 as those of the Florida Current since 1982¹¹ and the Greenland-Scotland ridge transports¹²
39 since the mid-1990s are some of the longest continuous ocean transport records available.
40 Continuous, full-depth, basinwide measurements of the Atlantic overturning circulation
41 only began in 2004 with the RAPID monitoring project at 26°N¹³. None of these records
42 are long enough to directly link ocean circulation with decadal climate variations such as
43 the AMO.

44

45 Sea-level measurements from tide gauges provide an integrated measure of water column
46 properties and offer timeseries of sufficient length (Ext. Data Fig. 1) to study decadal
47 ocean circulation variations. Investigating ocean circulation using tide gauges is not new:
48 the first attempt to estimate the Gulf Stream using tide gauges was made in 1938¹⁴. The
49 principle is based on geostrophic dynamics: on timescales longer than a few days, ocean
50 circulation is in geostrophic balance so, looking downstream, the sea level is seen to
51 increase from left to right in the northern hemisphere.

52

53 Estimates of the Gulf Stream using tide gauges have focused on the use of gauges on the
54 American east coast with an offshore estimate of sea level from either an island gauge¹⁵
55 or a reconstructed sea level¹⁶. A weakness of this method is that the offshore
56 measurement lies in the eddy-filled ocean where sea-level fluctuations at any one point
57 are influenced by the mesoscale¹⁷ even on long timescales, increasing the difficulty of
58 making estimates of ocean circulation that is coherent on large spatial scales. This is the
59 case for sea level at Bermuda, whose decadal fluctuations can be reproduced by
60 considering a Rossby wave response to wind forcing¹⁶. To make estimates of ocean
61 circulation that capture the fluctuations in large-scale circulation and less eddy variability,
62 measurements close to or on the western boundary are necessary¹⁸. We account for this
63 by focusing on the gradient of sea level along the US east coast. The mean dynamic sea
64 level decreases to the north along the east coast of the US (Fig. 1a) due to the transition
65 from subtropical to subpolar gyres. This dynamic gradient reflects a circulation that
66 contains elements not only of the Gulf Stream but also of cold, subpolar water from the
67 north, primarily associated with the overturning circulation¹⁹. Indeed, in model

68 simulations, this meridional gradient of sea level along this coast responds strongly to
69 declines in the Atlantic overturning circulation²⁰. Ultimately, it is the heat transport that
70 we are interested in. And while the overturning circulation carries about 90% of the heat
71 at subtropical latitudes²¹, at the latitude of the intergyre region, ocean heat transport
72 consists of similar contributions from both overturning and gyre²². For this reason, we do
73 not discuss separately overturning and gyre but only ocean circulation in this intergyre
74 region, which contains elements of both mechanisms.

75

76 Sea-level fluctuations from Florida to Boston divide into two coherent groups either side
77 of Cape Hatteras²³ (Ext. Data Fig. 2, 3). This large-scale coherence in sea level is driven
78 by ocean circulation. North of Cape Hatteras, coherent sea-level fluctuations have been
79 linked with fluctuations in the overturning circulation^{19,24}. South of Cape Hatteras,
80 fluctuations in the Gulf Stream from Florida to Cape Hatteras are reflected in sea-level
81 fluctuations. As Cape Hatteras marks the boundary between the subtropical and subpolar
82 gyres on this coastline (Fig. 1a), we can construct a single sea-level composite
83 representative of the subtropical (subpolar) circulation by averaging sea-level from
84 linearly detrended, deseasonalised tide gauges, with the inverse barometer effect removed,
85 south (north) of the Cape (Fig. 1b, c). The difference, south minus north (Fig. 1d),
86 represents our circulation index. This index projects onto observed surface velocities
87 during the satellite era in the intergyre region, with a positive index associated with more
88 northwards flow and a more northerly path of this circulation (Extended Data Fig. 4).
89 Similarly, in a high resolution ocean model, over timescales that contain both the cool
90 phase of the AMO in the 1970s²⁵ and the warm phase of the 1990s²⁶, the sea-level index

91 projects onto a similar pattern of circulation, with a positive index associated with more
92 northward heat transport (Ext. Data Fig. 5).

93

94 Ocean circulation is proportional to heat transport at both subtropical and subpolar
95 latitudes²². A number of recent studies (e.g. Bryden et al.²⁷) have emphasized the
96 dominant role of ocean heat transport in heat content changes, relating the accumulation
97 (in time) of heat transport to heat content. This suggests that the accumulation of our sea-
98 level index across Cape Hatteras, as a proxy for ocean circulation, can be related to ocean
99 heat content. The largest AMO signal is in the subpolar region (Fig. 1a), so we wish to
100 show that, as a measure of ocean circulation, our sea-level index is related to heat
101 transport into the subpolar gyre and consequently heat content changes there. Such a
102 mechanism is supported by our model where the sea-level index leads the heat transport
103 into the subpolar gyre at 40°N and, consequently, the heat content changes there (Ext.
104 Data Fig. 6).

105

106 While we do not have observations of heat transport, we can relate our sea-level index
107 directly to the heat content changes in the subpolar gyre since 1960. Fig. 2a shows the
108 accumulated sea-level index and a direct estimate of the heat content in the area and
109 depth weighted temperature anomaly in the top 500 m between 40°N and 60°N. Heat
110 content trends are similar throughout the upper 1000 m of the Atlantic, below which they
111 reverse due to the depth structure of the Atlantic overturning circulation. The cool
112 subpolar upper ocean of the 1970s and 1980s and subsequent warming in the 1990s is
113 captured by the accumulated sea-level index, observationally supporting the hypothesis

114 that circulation changes and not only air-sea fluxes were involved in these changes²⁸. For
115 the purposes of statistical analyses, the timeseries have had a 7-year low-pass, Tukey
116 filter applied to them, which is referred to with the prefix ‘7-year’ from here on. The 7-
117 year sea-level index leads the 7-year rate of heat content change by 2 years with a
118 maximum correlation of 0.58 (significant at the 95% level). Why the accumulated sea-
119 level index leads the large rise in heat content from 40°N to 60°N in the early 1990s can
120 be interpreted by looking at maps of the heat content anomaly evolution. Heat content
121 builds downstream of the intergyre region from the mid-1980s to the mid-1990s (Fig. 2b).
122 This heat content anomaly is then observed downstream in the subpolar gyre in the late
123 1990s and early 2000s (Fig. 2c), indicating that the sea-level index could provide an early
124 indication of subpolar heat content change.

125

126 The first mode of atmospheric variability over the North Atlantic, the NAO forces both
127 buoyancy and wind-driven ocean circulation⁷ and, we believe, is the major forcing of the
128 circulation in the intergyre region. The 7-year NAO is significantly correlated with
129 ($r=0.71$ at the 98% level) and leads the 7-year sea-level difference by approximately 1
130 year over the period 1950 to 2012. On extending the time period to 1920-2012, the
131 correlation drops slightly but is still significantly correlated ($r=0.61$ at the 98% level, Ext.
132 Data Fig. 7). The fact that the correlation between the sea-level difference and the NAO
133 is higher and more significant than the correlation of the NAO with either the southern or
134 northern sea-level (Fig. 1b, c) composites with the NAO ($r=-0.5$ at the 86% level for the
135 southern composite; $r=-0.43$ at the 70% level for the northern) supports our hypothesis
136 that the NAO forces the ocean circulation and consequently the ocean heat transport into

137 the subpolar gyre.

138

139 In the past 90 years, the AMO has undergone three major transitions: warming in the
140 mid-90s and 1920s, and a cooling in the 1960s. From the early-1920s, when the tide
141 gauge network along the east coast of North America was developed, robust comparisons
142 of our sea-level index to the AMO are possible (Fig. 3). The accumulated sea-level index
143 and the accumulated NAO are linearly detrended and capture much of the multi-decadal
144 variation. The 7-year sea-level index leads the 7-year rate of change of the AMO by 2
145 years and is significantly correlated ($r=0.51$, significant at the 96% level, Ext. Data Fig.
146 8). This lead time of 2 years remains consistent when the timeseries is broken into 60
147 year blocks. In recent years, the sea-level index (Fig. 1d) indicates that the AMO is again
148 transitioning to a negative phase, consistent with observations of a reduced overturning
149 circulation⁸.

150

151 Using the sea-level difference between subtropical and subpolar gyres, we have
152 developed and validated a proxy for ocean circulation in the intergyre region. This
153 represents a mechanism for ocean heat transport to the subpolar gyre and heat content
154 changes there. When observations exist, heat content changes have coincided with the
155 major phase transitions of the AMO, confirming that ocean circulation plays a key role in
156 decadal Atlantic variability. The ocean responds to NAO forcing with changes in ocean
157 circulation: on decadal timescales, the ocean integrates NAO forcing and returns it to the
158 atmosphere as the AMO. This is implicitly the Bjerknes compensation that had
159 previously been seen in air-sea fluxes²⁹. The sea-level difference provides an indicator of

160 ocean circulation changes that precede phase changes in the AMO, thus explaining why,
161 as the positive AMO declines⁴, sea-level rise is accelerating north of Cape Hatteras^{9,10}.
162 While Greenland ice sheet melt has been linked with accelerating sea-level rise in recent
163 years, the period of accelerated sea-level rise from the 1950s to the 1970s¹⁰ as well as the
164 current period coinciding with a declining AMO indicates that multi-decadal fluctuations
165 in ocean circulation play a key role. In this framework, sea-level rise along the US east
166 coast becomes entwined with the climate impacts of the AMO.

167

168 **References**

- 169 1. Zhang, R. & Delworth, T. L. (2006) Impact of Atlantic multidecadal oscillations on
170 India/Sahel rainfall and Atlantic hurricanes. *Geophysical Research Letters* 34,
171 L23708.
- 172 2. Sutton, R. T. & Dong, B. (2012) Atlantic Ocean influence on a shift in European
173 climate in the 1990s. *Nature Geoscience* 5, 788—792.
- 174 3. Goldenberg, S. B., Landsea, C. W., Mestas-Nuñez, A. M., & Gray, W. M. (2001) The
175 recent increase in Atlantic hurricane activity: Causes and implications. *Science* 293,
176 474—479.
- 177 4. Chen, X. & Tung, K.-K. (2014) Varying planetary heat sink led to global-warming
178 slowdown and acceleration. *Science* 345, 897—903.
- 179 5. Delworth, T. L. & Mann, M. E. (2000) Observed and simulated multidecadal
180 variability in the Northern Hemisphere. *Climate Dynamics* 16, 661—676.

- 181 6. Booth, B. B., Dunstone, N. J., Halloran, P. R., Andrews, T., & Bellouin, N. (2012)
182 Aerosols implicated as a prime driver of twentieth-century North Atlantic climate
183 variability. *Nature* 484, 228—232.
- 184 7. Marshall, J., Johnson, H., & Goodman, J. (2001) A study of the interaction of the
185 North Atlantic Oscillation with ocean circulation. *Journal of Climate* 14, 1399—
186 1421.
- 187 8. Smeed, D. A., McCarthy, G. D., Cunningham, S., Frajka-Williams, E., Rayner, D.,
188 Johns, W., Meinen, C., Baringer, M., Moat, B., Ducez, A., & Bryden, H. L. (2014)
189 Observed decline of the Atlantic Meridional Overturning Circulation 2004 to 2012.
190 *Ocean Science* 10, 39—38.
- 191 9. Sallenger Jr, A. H., Doran, K. S., & Howd, P. A. (2012) Hotspot of accelerated sea-
192 level rise on the Atlantic coast of North America. *Nature Climate Change* 2, 884—
193 888.
- 194 10. Boon, J. D. (2012) Evidence of sea level acceleration at US and Canadian tide
195 stations, Atlantic Coast, North America. *Journal of Coastal Research* 28, 1437—
196 1445.
- 197 11. Meinen, C. S., Baringer, M. O., & Garcia, R. F. (2010) Florida Current transport
198 variability: An analysis of annual and longer-period signals. *Deep Sea Research Part*
199 *I: Oceanographic Research Papers* 57, 835—846.
- 200 12. Østerhus, S., Turrell, W. R., Jónsson, S., & Hansen, B. (2005) Measured volume,
201 heat, and salt fluxes from the Atlantic to the Arctic Mediterranean. *Geophysical*
202 *Research Letters* 32, L07603.

- 203 13. McCarthy, G. D., Smeed, D. A., Johns, W. E., Frajka-Williams, E., Moat, B. I.,
204 Rayner, D., Baringer, M. O., Meinen, C. S., Collins, J., & Bryden, H. L. (2014)
205 Measuring the Atlantic Meridional Overturning Circulation at 26°N. *Progress in*
206 *Oceanography*, in press. [doi:10.1016/j.pocean.2014.10.006](https://doi.org/10.1016/j.pocean.2014.10.006)
- 207 14. Montgomery, R. (1938) Fluctuations in monthly sea level on eastern US coast as
208 related to dynamics of western North Atlantic Ocean. *Journal of Marine Research* 1,
209 165—185.
- 210 15. Iselin, C. O. (1940) Preliminary report on long-period variations in the transport of
211 the Gulf Stream system. *Papers in Physical Oceanography and Meteorology* 3, 1.
- 212 16. Sturges, W. & Hong, B. (1995) Wind forcing of the Atlantic thermocline along 32 N
213 at low frequencies. *Journal of physical oceanography* 25, 1706—1715.
- 214 17. Wunsch, C. (2008) Mass and volume transport variability in an eddy-filled ocean.
215 *Nature Geoscience* 1, 165-168.
- 216 18. Kanzow, T., Johnson, H., Marshall, D., Cunningham, S., Hirschi, J.-M., Mujahid, A.,
217 Bryden, H., & Johns, W. (2009) Basinwide integrated volume transports in an eddy-
218 filled ocean. *Journal of Physical Oceanography* 39, 3091—3110.
- 219 19. Bingham, R. J. & Hughes, C. W. (2009) Signature of the Atlantic meridional
220 overturning circulation in sea level along the east coast of North America.
221 *Geophysical Research Letters* 36, L02603.
- 222 20. Yin, J., Schlesinger, M. E., & Stouffer, R. J. (2009) Model projections of rapid sea-
223 level rise on the northeast coast of the United States. *Nature Geoscience* 2, 262—266.

- 224 21. Johns, W. E., Baringer, M. O., Beal, L. M., Cunningham, S. A., Kanzow, T., Bryden,
225 H. L., Hirschi, J. J. M., Marotzke, J., Meinen, C. S., Shaw, B., & Curry, R. (2011)
226 Continuous, Array-Based Estimates of Atlantic Ocean Heat Transport at 26.5°N.
227 *Journal of Climate* 24, 2429—2449.
- 228 22. Grist, J. P., Josey, S. A., Marsh, R., Good, S. A., Coward, A. C., De Cuevas, B. A.,
229 Alderson, S. G., New, A. L., & Madec, G. (2010) The roles of surface heat flux and
230 ocean heat transport convergence in determining Atlantic Ocean temperature
231 variability. *Ocean dynamics* 60, 771—790.
- 232 23. Thompson, P. & Mitchum, G. (2014) Coherent sea level variability on the North
233 Atlantic western boundary. *Journal of Geophysical Research: Oceans*, 119,
234 doi:10.1002/2014JC009999.
- 235 24. Ezer, T. (2013) Sea level rise, spatially uneven and temporally unsteady: why the US
236 east coast, the global tide gauge record and the global altimeter data show different
237 trends. *Geophysical Research Letters*, 40,1—6.
- 238 25. Hodson, D. L., Robson, J. I., & Sutton, R. T. (2014) An Anatomy of the Cooling of
239 the North Atlantic Ocean in the 1960s and 1970s. *Journal of Climate* 27, 8229—
240 8243.
- 241 26. Häkkinen, S. & Rhines, P. B. (2004) Decline of subpolar North Atlantic circulation
242 during the 1990s. *Science* 304, 555—559.
- 243 27. Bryden, H. L., King, B. A., McCarthy, G. D., & McDonagh, E. L. (2014) Impact of a
244 30% reduction in Atlantic meridional overturning during 2009-2010. *Ocean Science*
245 10, 683-691.

246 28. Robson, J., Sutton, R., Lohmann, K., Smith, D., & Palmer, M. D. (2012) Causes of
247 the rapid warming of the North Atlantic Ocean in the mid-1990s. *Journal of Climate*
248 25, 4116—4134.

249 29. Gulev, S., Latif, M., Keenlyside, N. S., & Koltermann, K. (2013) North Atlantic
250 Ocean Control on Surface Heat Flux at Multidecadal Timescale. *Nature* 499, 464—
251 467.

252

253 **Supplementary Information**

254 Matlab© code and comma-separated data used in the manuscript are available to
255 download from <http://bit.ly/1F7gtps>.

256

257 **Acknowledgements**

258 GDM and DAS are supported by UK Natural Environment Research Council (NERC)
259 RAPID-WATCH program. IDH was partly supported by the UK NERC consortium
260 project iGlass (NE/I009906/1). JPG and JJMH are supported by NERC National
261 Capability funding.

262

263 **Author contributions**

264 GDM originated and developed the concept. IDH provided the tide gauge data analysis.
265 JPG and JJMH provided the numerical model analysis. DAS carried out the statistical
266 analysis. All authors contributed to the shaping and production of the manuscript

267

268

269 **Author information**

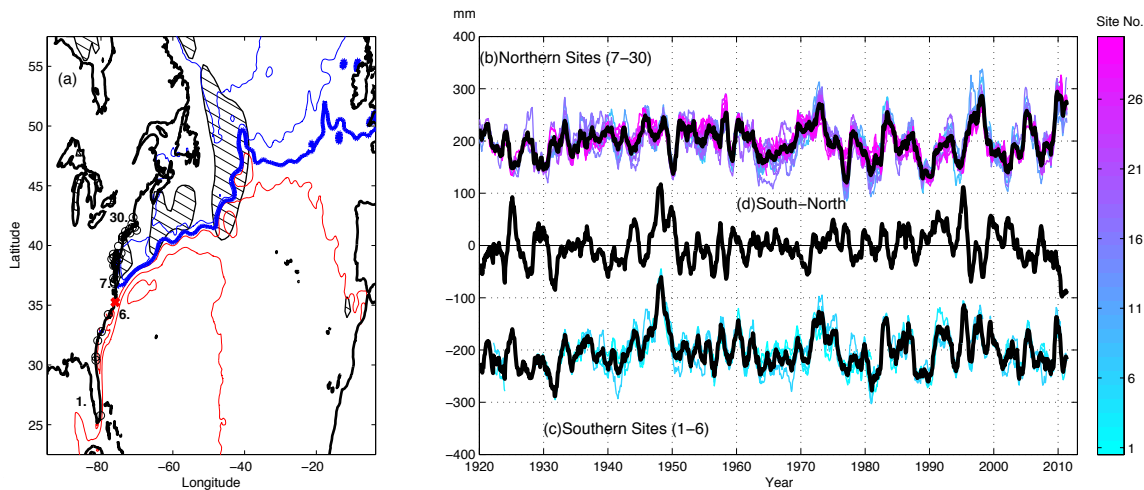
270 Reprints and permissions information is available at www.nature.com/reprints. The

271 authors declare no competing financial interests. Correspondence and requests for

272 materials should be addressed to Gerard McCarthy (gerard.mccarthy@noc.ac.uk).

273

274 **Figure Legends**



276 **Figure 1: Dynamic sea-level and circulation along the western Atlantic seaboard. (a)**

277 Negative (positive) mean dynamic topography contours (m) in blue (red) indicate

278 cyclonic (anticyclonic) geostrophic streamlines. The zero contour (dark blue) marks the

279 boundary between the subtropical and subpolar gyres. Hatched areas indicate warm SST

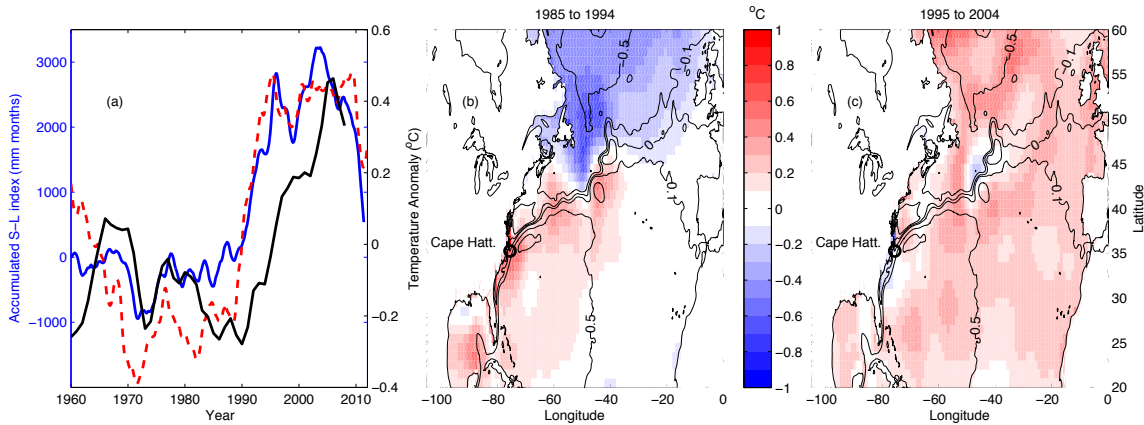
280 anomalies of greater than 0.5°C during the positive phase of the AMO from 1995-2004

281 relative to from 1961-2012. Dynamic sea-level anomalies (b) north (sites 7—30, +200

282 mm offset) and (c) south (sites 1—6, -200 mm offset) of Cape Hatteras, with averages in

283 black. (d) The difference in sea-level, southern minus northern average, defines our sea-

284 level index for ocean circulation.



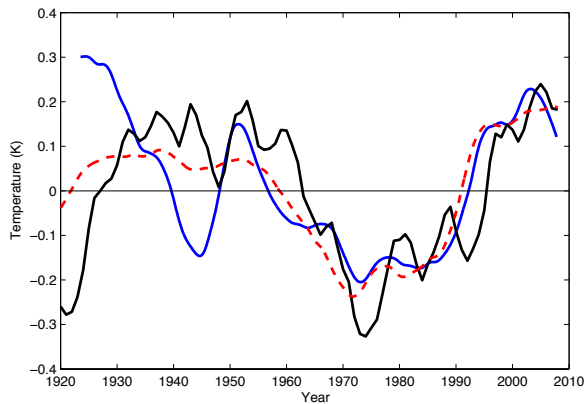
285

286 **Figure 2: Relating the sea-level circulation index to heat content changes. (a)**

287 Accumulated sea-level index (nominally, in mm month) derived from accumulating the
 288 sea-level circulation index (blue), temperature anomaly in the upper 500 m of the
 289 subpolar North Atlantic from 40° to 60°N (black) and accumulated NAO (red, dashed).

290 (b) Average temperature anomaly in the top 500 m for the periods 1985-1994 relative to
 291 the average from 1958-2010. Contours of mean dynamic topography defined in Fig. 1a

292 are overlaid for reference. (c) Same as (b) but for the period 1995-2004.



293

294 **Figure 3: Sea-level circulation indices, the NAO and the AMO on multi-decadal**

295 **timescales.** Accumulated sea-level index (blue), which is representative of subpolar heat
 296 content evolution, accumulated NAO (red, dashed) and AMO (black). The heat content
 297 proxy and the accumulated NAO have been normalised. All timeseries have been 7-year

298 low-pass filtered. The accumulated sea-level index and accumulated NAO have been
299 detrended.

300

301 **Methods**

302 *Data*

303 Monthly mean sea-level records were obtained from the Permanent Service for Mean
304 Sea-level (www.psmsl.org) for tide gauges stretching from Florida to Boston (Locations
305 1 to 30, Ext. Data Fig. 1). Linear trends were removed from each record. This removes
306 the impact of Glacial Isostatic Adjustment and other land subsidence effects, which have
307 time periods of thousands of years and are known to affect tide gauges along this
308 coastline. A 12-month low-pass filter removed the seasonal cycle. Southern (northern)
309 composites of sea level we calculated by averaging records 1-6 (7-30). The meridional
310 coherence of sea-level fluctuations is such, that using just a single tide gauge results in an
311 rms error of only 5 mm relative to the full composite. Finally, the sea-level index is
312 simply the difference obtained by subtracting the northern from the southern sea-level
313 composite. The high level of meridional coherence allows the interpretation of the sea-
314 level gradient as this simple index.

315

316 Monthly NAO data from the National Center for Atmospheric Research "The Climate
317 Data Guide: Hurrell North Atlantic Oscillation (NAO) Index (PC-based)"
318 ([https://climatedataguide.ucar.edu/climate-data/hurrell-north-atlantic-oscillation-nao-](https://climatedataguide.ucar.edu/climate-data/hurrell-north-atlantic-oscillation-nao-index-pc-based)
319 [index-pc-based](https://climatedataguide.ucar.edu/climate-data/hurrell-north-atlantic-oscillation-nao-index-pc-based)); monthly AMO index, based on the Kaplan SST dataset (from
320 <http://www.esrl.noaa.gov/psd/data/timeseries/AMO/>); subsurface temperature data from

321 the EN3 product (<http://www.metoffice.gov.uk/hadobs/en3/>); geostrophic velocity
322 anomalies, were produced and distributed by Aviso (<http://www.aviso.altimetry.fr/>), as
323 part of the Ssalto ground processing segment. CNES-CLS09 Mean Dynamic Topography
324 (v1.1 release) for the period 1993-1999 was produced by the French Space Agency
325 CNES.

326

327 *Model validation*

328 The multi-decadal oscillation of SSTs is most intense in the subpolar gyre (Fig. 1a).
329 Modelling studies have shown that it is ocean heat transport into the subpolar gyre (here
330 we choose 40°N) that controls the heat content of the subpolar upper ocean and
331 consequently the SST. The concept here is that circulation in the intergyre region reflects
332 the balance between warm subtropical water entering the subpolar gyre and colder
333 subpolar water being recirculated within the gyre. We show that the sea-level gradient
334 along the US east coast is a good proxy for this circulation (Ext. Data Fig. 4 and 5).

335 We can relate sea-level changes to ocean circulation in a reduced gravity
336 geostrophic framework:

$$\mathbf{v} = \frac{\mathbf{g}'}{f} \mathbf{k} \times \nabla h,$$

337 where \mathbf{v} is geostrophic velocity, \mathbf{k} is the unit vector in the vertical direction, h is sea
338 level, \mathbf{g}' is reduced gravity and f is the Coriolis parameter. To estimate the transport in
339 the intergyre region, previous studies have considered the sea-level difference between an
340 onshore tide gauge and an offshore tide gauge, such as Bermuda. Ezer (2013)²⁴, for
341 example, relates the sea-level difference between Atlantic City and Bermuda to the
342 Atlantic overturning circulation.

343

344 However, Bermuda is in the eddy-filled ocean interior¹⁷, which can disrupt spatially-
345 coherent ocean transport signals. Our approach is to use sea-level estimates south of Cape
346 Hatteras instead of an offshore sea-level estimate. Dynamic topography along the US east
347 coast also decreases to the north across the intergyre boundary at Cape Hatteras much as
348 it decreases from Bermuda to Atlantic City. However, measurements on the coast do not
349 suffer the same contamination due to eddies as mid-ocean measurements¹⁸. Hence we
350 estimate the transport along the intergyre boundary as:

$$v_{ig} \approx h_s - h_n,$$

351 where the subscript *ig* refers to the intergyre region, *s* and *n* refer to south and north
352 respectively. We can formulate the heat transport through a section straddling the
353 intergyre boundary as:

$$HT_{ig} = \rho c_p \iint \Theta v_{ig} dA,$$

354 where ρ is density, c_p is specific heat capacity of seawater, Θ is conservative temperature
355 and A is the area of the section considered. In this study we assume that the velocity
356 fluctuations dominate the temperature fluctuations and so set the heat transport directly
357 proportional to the intergyre velocity. This is an assumption that has proved true in direct
358 heat transport estimates²¹. We note there is no dilemma in picking the location of the
359 northern or southern points as the meridional coherence of sea level fluctuations allows
360 us to use a simple average of all sea level records from Miami Beach to Cape Hatteras
361 (Cape Hatteras to Boston) for h_s (h_n).

362 In terms of upper ocean heat content, the heat transported in this intergyre region
363 has a profound impact on the subpolar gyre. This is because warm water may be

364 transferred from the upper waters of the subtropics to the subpolar gyre whereas subpolar
365 water can only enter the subtropics at depth (traditionally in the deep western boundary
366 current). Therefore we relate the heat transport into the subpolar gyre and heat content of
367 the upper waters of the subpolar gyre to the transport in the intergyre region:

$$HT_{40^{\circ}\text{N}} \approx h_s - h_n.$$

368 For exactly the reason that we need to use tide gauges as a proxy for heat
369 transport, we cannot validate the conceptual model directly due to the lack of direct
370 observations. However, a global eddy-permitting ($1/4^{\circ}$) ocean model (ORCA-025) model
371 provides the framework to investigate these balances. The heat transport into the subpolar
372 gyre has previously been shown in this model to be the dominant factor in setting upper
373 ocean temperature in the subpolar gyre²². Here, we reproduce this result, showing that the
374 accumulated heat transport across 40°N captures the major decadal fluctuations in heat
375 content of the subpolar gyre (Ext. Data Fig. 6). We can use these heat transport
376 measurements to validate our circulation index. At this resolution there are shortcomings
377 in the representation of the Gulf Stream path: the Gulf Stream overshoots at Cape
378 Hatteras and separates from the US coast too far north. However, we take account of this
379 in choosing the northern and southern sea-level points so that they straddle the separation
380 point. Also, despite the model being eddy-permitting rather than eddy-resolving, it does
381 generate mesoscale variability. This is seen when including an offshore sea-level
382 measurement (such as Bermuda) in a sea-level circulation index. Such an index fails to
383 reflect the large scale circulation. This effect would be expected to be even larger in an
384 eddy-resolving model. Ext. Data Fig. 5 shows that the model-derived sea-level index
385 projects onto the intergyre velocities in a similar manner to the observed sea-level index.

386 Ext. Data Fig. 6 shows the accumulated sea-level difference compared with the
387 accumulated heat transport across a section near 40°N and the volume averaged
388 temperature of the upper 500 m of the subpolar gyre (40°N to 60°N). The sea-level
389 difference is significantly correlated with the heat transport into the subpolar gyre
390 ($r=0.62$) and leads by 5 years (as in the main text, we report statistics on unaccumulated
391 timeseries).

392

393 *Statistical analysis*

394 Cross-correlations are calculated using annually averaged data after first removing the
395 mean and linear trend from each variable. Two approaches are used to quantify the
396 uncertainty in the correlation. Firstly, we calculated the parameter

$$T = \sqrt{(N - 2)} \frac{r}{\sqrt{1 - r^2}},$$

397 where r is the correlation and N is the number of samples. The distribution of T is
398 assumed to have a t-distribution with $N-2$ degrees of freedom when the samples are not
399 autocorrelated. This is used with a one-sided test to estimate the likelihood that the
400 correlation has not occurred by chance (i.e. the certainty with which we can reject the
401 null hypothesis). Our data are autocorrelated and the number of independent samples
402 (degrees of freedom) is therefore smaller than N . To calculate the effective number of
403 degrees of freedom we follow Bretherton et al.³⁰ by evaluating the autocorrelation of each
404 variable and the estimate N as

$$N_{\text{eff}} = N_{\text{obs}} \frac{(1 - a_1 a_2)}{(1 + a_1 a_2)}$$

405 where N_{eff} is the degrees of freedom, N_{obs} is the number of observations and a_1, a_2 are the

406 values of the autocorrelations at a lag of one year. We evaluated N_{eff} over the longest
407 time for each variable and then used the lowest value for all correlations. For the shorter
408 time series N_{eff} was reduced in proportion to the length of the series. Degrees of freedom
409 are reported in Extended Data Table 1.

410

411 In a second approach we applied the non-parametric method described by Ebisuzaki³¹. A
412 large number (we used 10,000) of simulated time series are constructed from the Fourier
413 transform of one of the original data series by preserving the modulus of each Fourier
414 component but changing the phase to a random value between 0 and 2π . The distribution
415 of correlations between these random series and the second variable was then calculated.
416 The percentage of simulated correlations that are less than the observed correlation
417 indicates the confidence that the true correlation is greater than zero. Because we are
418 considering lagged correlations we modify the technique of Ebisuzaki³¹ so that for each
419 simulated time series we evaluate the maximum of cross-correlation across all lags rather
420 than the correlation at zero lag only. This provides a more stringent test of confidence.

421

422 To estimate the uncertainty in the time lag of the maximum correlation we used the times
423 at which the correlation was equal to the maximum value less the standard deviation of
424 correlations derived from the simulated time series. The results are summarized in
425 Extended Data Table 1.

426

427 We have also evaluated the correlation over shorter periods to determine if the lag has
428 remained constant over time. Results from three overlapping 60-year periods are shown

429 in Ext. Data Table 2. For each the correlation is a maximum when sea-level difference
430 leads the differentiated AMO by 2 to 3 years.

431

432 The text refers to both accumulated and unaccumulated timeseries. Accumulation of zero
433 mean timeseries constrains the beginning and end of the accumulated timeseries to zero.

434 To avoid this arbitrary constraint, we report all our statistics on unaccumulated timeseries.

435 As mentioned, for the purposes of statistical analyses, the timeseries have had a 7-year,

436 Tukey filter applied to them, which is referred to in the text with the prefix ‘7-year’ in the

437 text.

438

439 **Methods References**

440 30. Bretherton, C. S., Widmann, M., Dymnikov, V. P., Wallace, J. M., & Bladé, I. (1999)

441 The effective number of spatial degrees of freedom of a time-varying field. *Journal of*

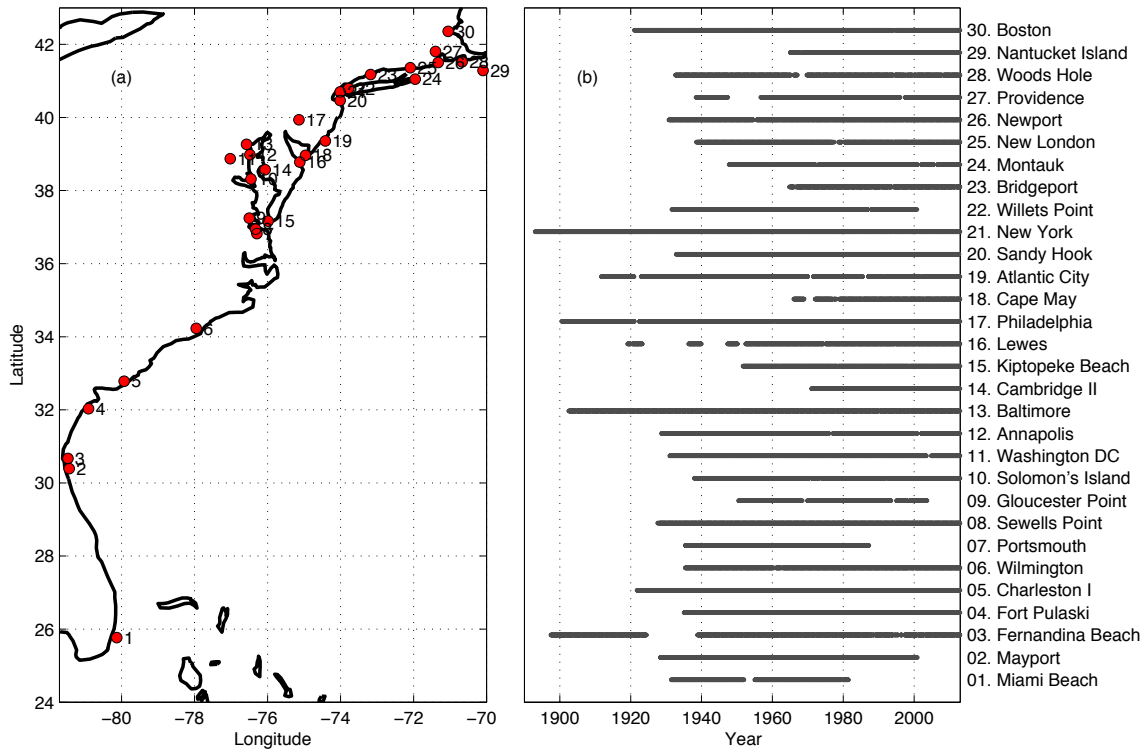
442 *Climate* 12, 1990—2009.

443 31. Ebisuzaki, W. (1997) A method to estimate the statistical significance of a correlation

444 when the data are serially correlated. *Journal of Climate* 10, 2147—2153.

445

446 **Extended Data Legends**



447

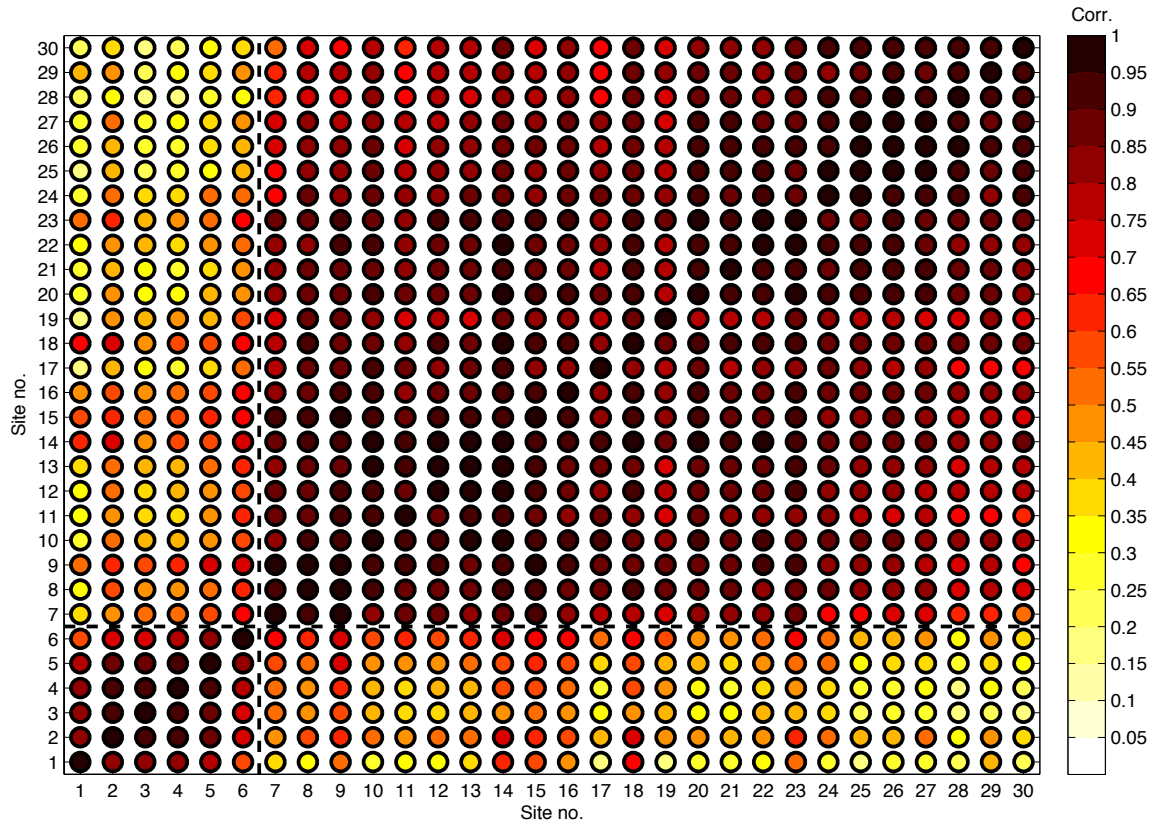
448 **Extended Data Figure 1: Tide gauges used in this study. (a) Locations and (b)**

449 temporal coverage of the tide gauges used in this study.



450

451 **Extended Data Figure 2: Dynamic sea-level anomalies from the 30 stations used in**
 452 **this study.** Linear trends were removed from each record. This removes the impact of
 453 Glacial Isostatic Adjustment and other land subsidence effects, which have time periods
 454 of thousands of years and are known to affect tide gauges along this coastline. A seasonal
 455 cycle was removed using a 12-month boxcar filter. From 1920, there are multiple tide
 456 gauges both north and south of Cape Hatteras so this is when we begin our study.

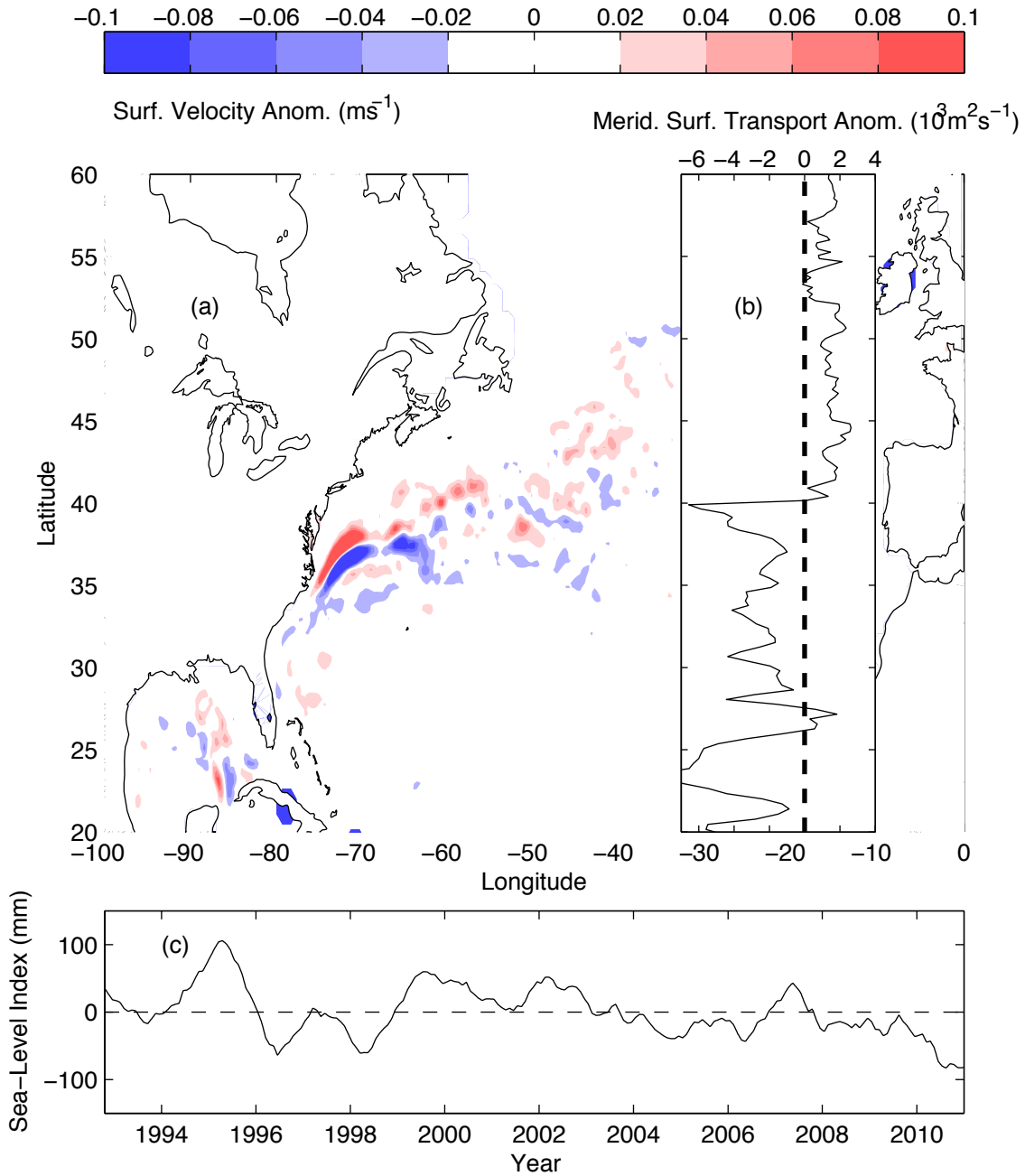


457

458 **Extended Data Figure 3: Correlation of tide gauges along the US east coast relative**

459 **to one another.** The dashed line indicates the location of Cape Hatteras. There is high

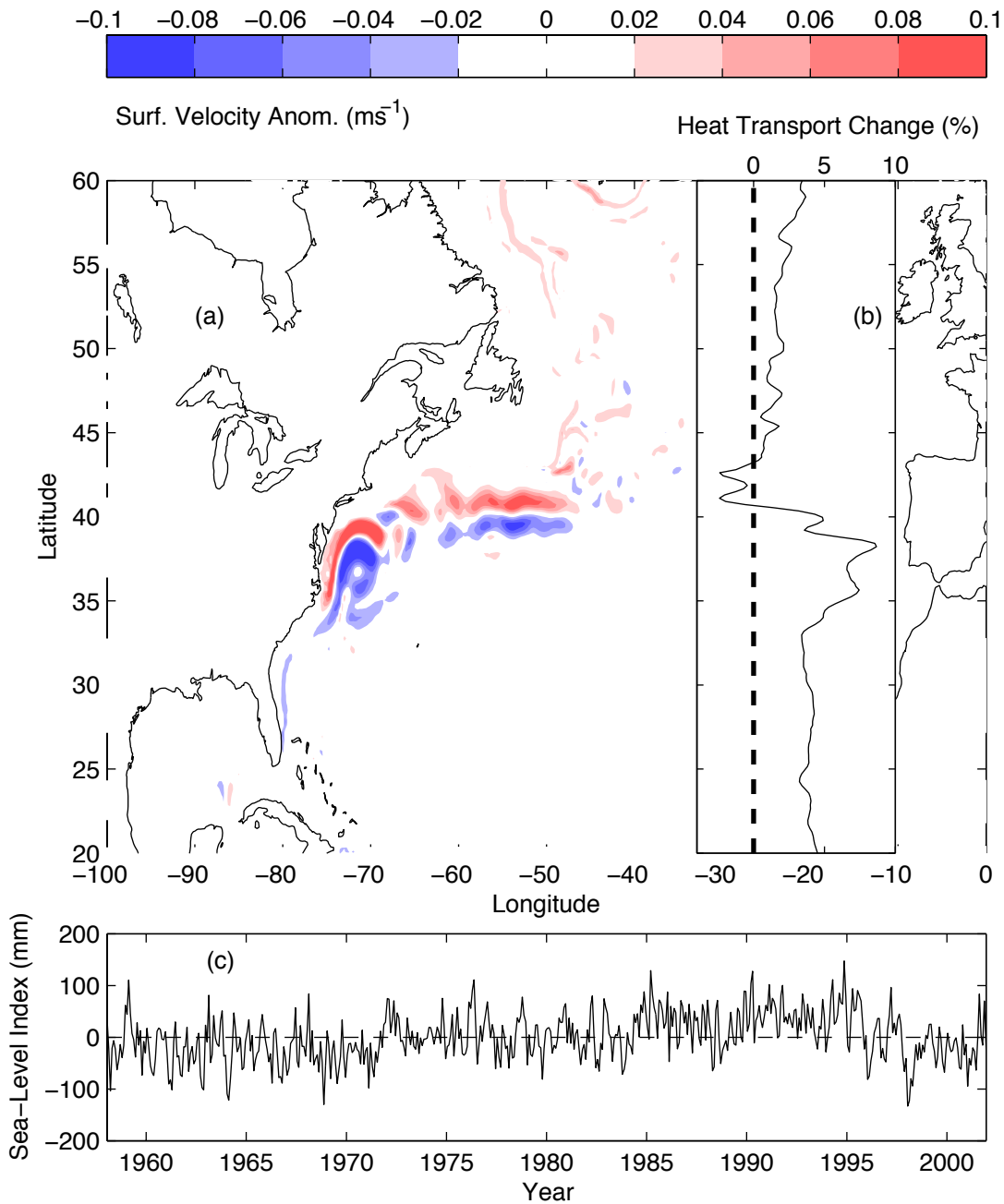
460 correlation between tide gauges grouped north and south of Cape Hatteras.



461

462 **Extended Data Figure 4: Surface velocity anomaly when the sea-level index is**
 463 **positive.** (a) Magnitude (ms^{-1}) and (b) zonally integrated meridional velocity anomalies
 464 ($10^3 \text{ m}^2 \text{ s}^{-1}$) for the time period 1993 to 2011, corresponding to when (c) the sea-level
 465 index is positive. A positive sea-level index is associated with a more northerly
 466 circulation in the intergyre region and increased surface flow into the subpolar gyre.

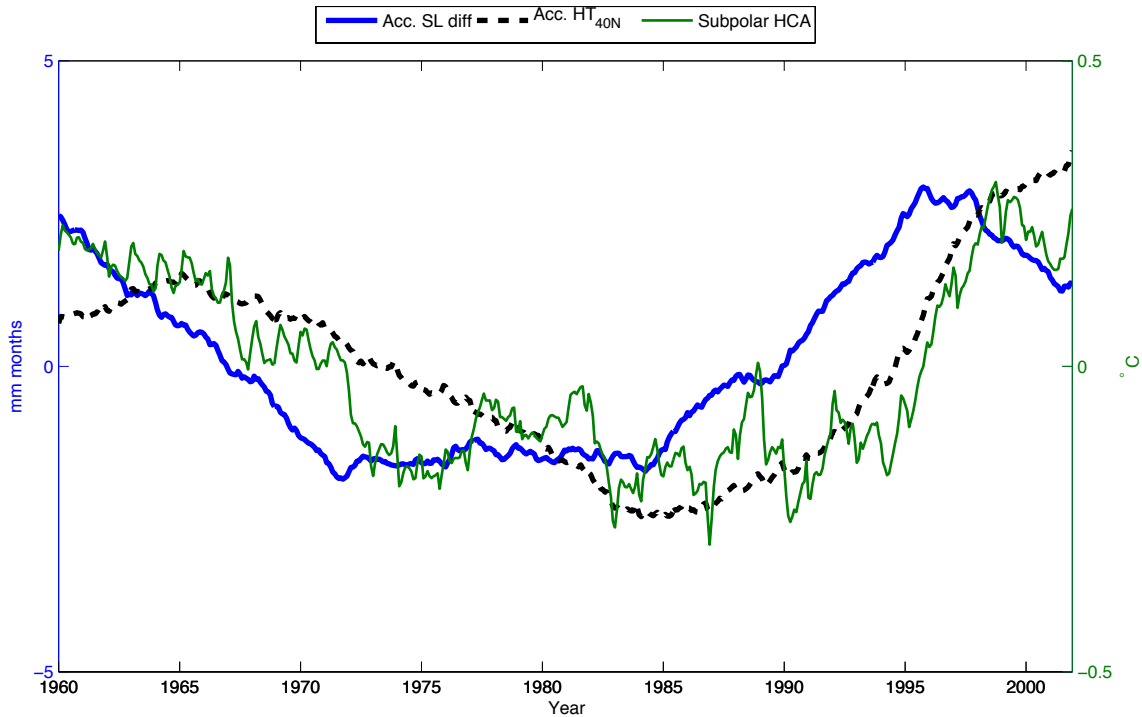
467 Velocities are geostrophic surface velocities derived from satellite altimetry.



468

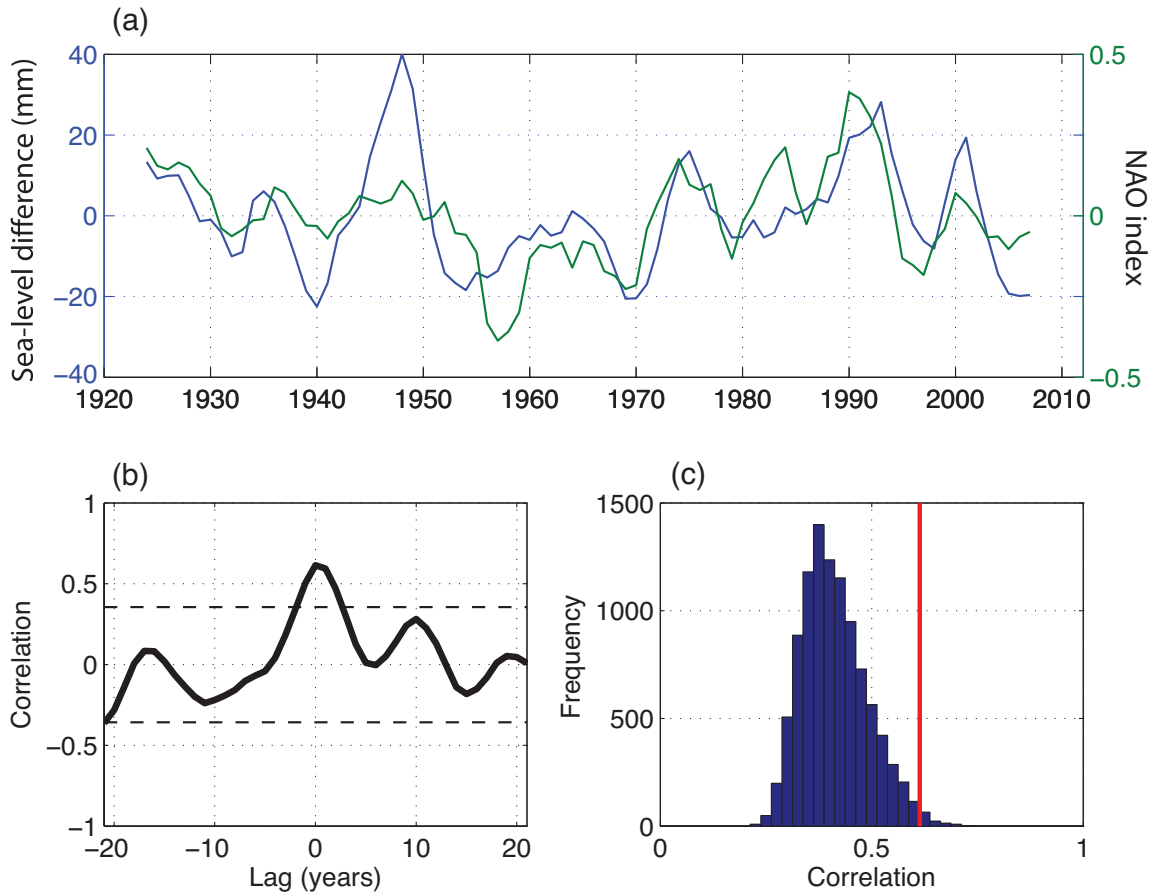
469 **Extended Data Figure 5: Model-derived surface velocity anomaly magnitude when**
470 **the model-based sea-level index is positive.** Similar to observed velocities, positive
471 indices are associated with more northerly circulation in the intergyre region. (a) Surface
472 velocity magnitude (ms^{-1}) and (b) percentage of meridional heat transport change (%) for

473 the time period 1958 to 2001, corresponding to when (c) the model-derived sea-level
474 index is positive. Similar to the satellite observations, a positive sea-level index is
475 associated with a more northerly circulation in the intergyre region. Meridional heat
476 transport change in both subtropical and subpolar gyres is positive when the sea-level
477 index is positive.



478

479 **Extended Data Figure 6: Model-derived sea-level index, heat transport and**
480 **subpolar heat content.** The accumulated sea-level index (blue, mm months) leads the
481 accumulated heat transport into the full subpolar gyre across section approximately 40°N
482 (black, normalized units). The heat transport into the subpolar gyre dominates the top 500
483 m temperature anomaly (green, °C) in the subpolar gyre.



484

485 **Extended Data Figure 7: Relationship between sea-level index and the NAO.** (a) 7-

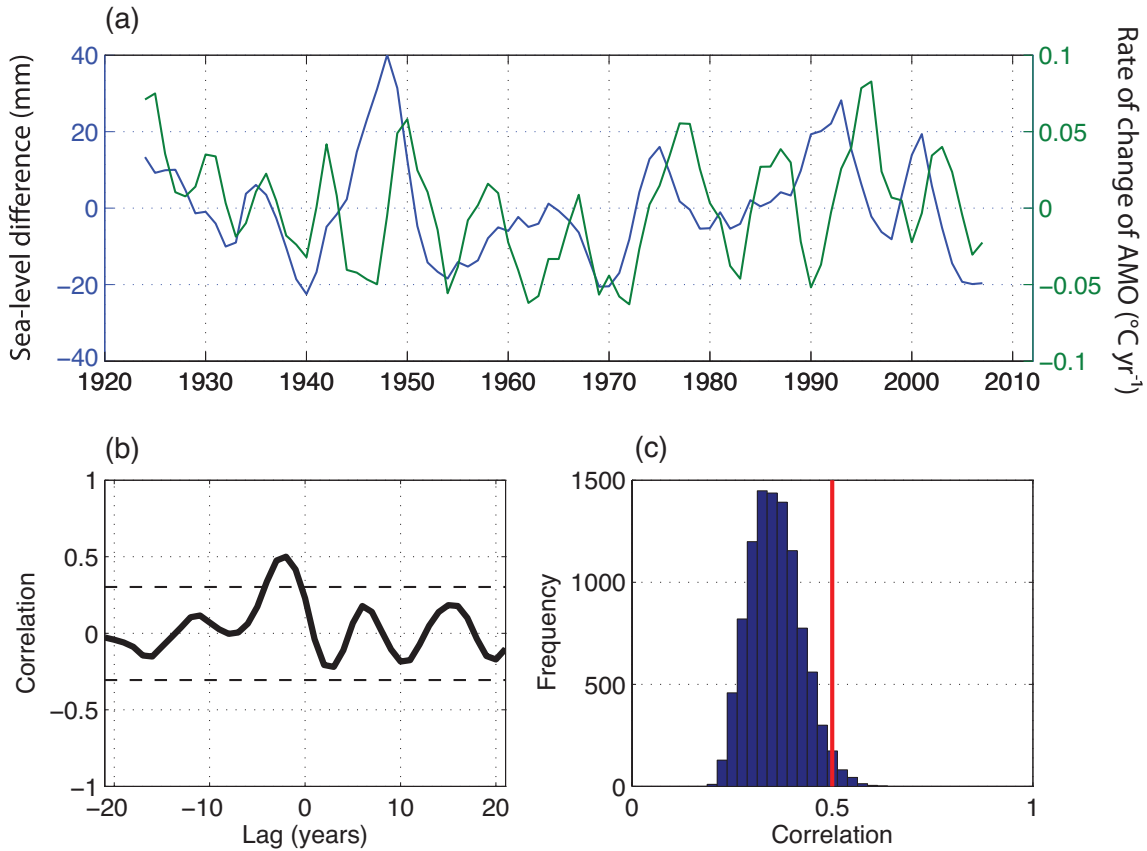
486 year sea level difference (blue, cm) and 7-year NAO (green, normalized units). (b)

487 Lagged correlations between the two quantities. (c) Scrambled correlation tests. The

488 histogram indicates the typical correlations that would be expected from randomly

489 generated timeseries with similar spectral properties to the original timeseries. The red

490 line indicates the maximum correlation between the two timeseries.



491

492 **Extended Data Figure 8: Relationship between sea-level index and the rate of**
 493 **change of the AMO.** (a) 7-year sea level difference (blue) and rate of change of the
 494 AMO (green). (b) Lagged correlations between the two quantities. (c) Scrambled
 495 correlation tests. The histogram indicates the typical correlations that would be expected
 496 from randomly generated timeseries with similar spectral properties to the original
 497 timeseries. The red line indicates the maximum correlation between the two timeseries.

498

Var X	Var Y	Filt (yrs)	Time interval	DoF	Corr	Sig. % (t-stat)	Sig. % (Scrm)	RMS of rand corr	Lag at max corr (yrs)	Estimate d range of lag (yrs)
B-A	Di HC	7	1950-2012	9	0.58	95	98	0.22	-2	-3 to 0
B-A	NAO	7	1950-2012	9	0.71	98	98	0.29	1	-1 to 2
NAO	Di HC	7	1950-2012	9	0.41	86	84	0.18	-2	-4 to -1
B-A	NAO	7	1920-2012	13	0.61	98	99	0.21	0	-1 to 2
B	NAO	7	1920-2012	13	-0.50	95	86	0.23	-11	-13 to 7
A	NAO	7	1920-2012	13	-0.43	91	70	0.22	1	-3 to 4
B-A	Di AMO	7	1920-2012	13	0.51	96	98	0.18	-2	-4 to -1
NAO	Di AMO	7	1920-2012	13	0.58	98	98	0.21	-4	-5 to -2

500

501 **Extended Data Table 1: Correlation, lags and significance of sea-level, NAO and**
 502 **rates of change of the AMO. B (A) is the southern (northern) sea-level index. Di refers**
 503 **to the rate of change. HC refers to subpolar heat content from 40° to 60°N.**

From	To	Correlation	Lag (yrs)	Lag range (yrs)
1920	2012	0.5	-2	-4 to -1
1920	1980	0.36	-1	-3 to 0
1936	1995	0.46	-3	-4 to -1
1952	2012	0.54	-2	-4 to 0

504

505 **Extended Data Table 2: Correlation, lags and lag range of sea-level index and the**
 506 **rate of change of the AMO over various time periods to investigate the consistency**
 507 **of the lags.**

508